MITSUBISHI ELECTRIC RESEARCH LABORATORIES
https://www.merl.com

Continuous-Time Successive Convexification for Passively-Safe Six-Degree-of-Freedom Powered-Descent Guidance

Elango, Purnanand; Vinod, Abraham P.; Di Cairano, Stefano; Weiss, Avishai

TR2025-008 January 08, 2025

Abstract

We present an optimization-based method for the fuel-optimal powered descent of a six-degree-of-freedom (6-DoF) lander while ensuring passive safety for a specified duration with respect to an avoid set near the landing site. In other words, the ballistic trajectory of the vehicle, in the event of unplanned engine failure, does not enter an avoid set (e.g., containing critical infrastructure) for a specified time horizon. The proposed solution method leverages the recently introduced CT-SCVX framework, wherein the set-based passive-safety constraint is subjected to an isoperimetric reformulation. The resulting free- final-time optimal control problem is solved through: 1) time-dilation, 2) multiple-shooting discretization, 3) l1-exact penalization of nonconvexities, and 4) the prox-linear method, which is a convergence-guaranteed sequential convex programming (SCP) algorithm for convex-composite minimization. The proposed approach eliminates the commonly encountered inter-sample constraint violation without the need for computationally expensive mesh-refinement heuristics; i.e., we can generate a high-fidelity feasible solution on coarse discretization grids. We provide a numerical demonstration of the proposed approach on a realistic lunar-landing example.

AIAA SciTech 2025

Mitsubishi Electric Research Laboratories, Inc.
201 Broadway, Cambridge, Massachusetts 02139

Continuous-Time Successive Convexification for Passively-Safe Six-Degree-of-Freedom Powered-Descent Guidance

Purnanand Elango*, Abraham P. Vinod†, Stefano Di Cairano‡, and Avishai Weiss§
Mitsubishi Electric Research Laboratories, Cambridge, MA, 02139, USA

We present an optimization-based method for the fuel-optimal powered descent of a six-degree-of-freedom (6-DoF) lander while ensuring passive safety for a specified duration with respect to an avoid set near the landing site. In other words, the ballistic trajectory of the vehicle, in the event of unplanned engine failure, does not enter an avoid set (e.g., containing critical infrastructure) for a specified time horizon. The proposed solution method leverages the recently introduced CT-SCvx framework, wherein the set-based passive-safety constraint is subjected to an isoperimetric reformulation. The resulting free-final-time optimal control problem is solved through: 1) time-dilation, 2) multiple-shooting discretization, 3) ℓ_1-exact penalization of nonconvexities, and 4) the prox-linear method, which is a convergence-guaranteed sequential convex programming (SCP) algorithm for convex-composite minimization. The proposed approach eliminates the commonly encountered inter-sample constraint violation without the need for computationally expensive mesh-refinement heuristics; i.e., we can generate a high-fidelity feasible solution on coarse discretization grids. We provide a numerical demonstration of the proposed approach on a realistic lunar-landing example.

Notation

$\mathbb{R}^n$	set of real $n \times 1$ vectors
$\mathbb{R}^{n\times m}$	set of real $n \times m$ matrices
0_n	vector of zeros in $\mathbb{R}^n$
$0_{n\times m}$	matrix of zeros in $\mathbb{R}^{n\times m}$
1_n	vector of ones in $\mathbb{R}^n$
e_k^n	unit-vector in $\mathbb{R}^n$ where the kth element is 1
(a, b)	concatenation of vectors $a \in \mathbb{R}^n$ and $b \in \mathbb{R}^m$ to form a vector in $\mathbb{R}^{n+m}$
$[A\ B]$	concatenation of matrices $A \in \mathbb{R}^{n\times m_1}$ and $B \in \mathbb{R}^{n\times m_2}$ to form a matrix in $\mathbb{R}^{n\times(m_1+m_2)}$
$a \leq b$	$a_i \leq b_i$ for each $1 \leq i \leq m$, where $a = (a_1, \ldots, a_m) \in \mathbb{R}^m$ and $b = (b_1, \ldots, b_m) \in \mathbb{R}^m$
$\mathrm{sdist}_C(z)$	signed distance of vector $z \in \mathbb{R}^n$ to set $C \subset \mathbb{R}^n$
$\|z\|$	Euclidean norm of vector z
$\|z\|_+$	$\max\{0, z\}$ (applied elementwise if z is not a scalar)
$\|z\|_+$	$\|(\|z_1\|_+, \ldots, \|z_n\|_+)\|$, where $z = (z_1, \ldots, z_n) \in \mathbb{R}^n$
$\nabla_j F(v_1, \ldots, v_m)$	partial derivative of F with respect to its jth argument, evaluated at $v_1, \ldots, v_m$, where $1 \leq j \leq m$
$\nabla F(x)$	$\nabla_1 F(x)$

*Research Scientist
†Principal Research Scientist
‡Distinguished Research Scientist
§Senior Principal Research Scientist

I. Introduction

The renewed interest in space exploration missions, with an emphasis on satisfying safety- and performance-critical constraints, has recently brought attention to optimization-based methods for trajectory generation [1], [2, Sec. 3.1]. In particular, much attention is focused on powered-descent guidance (PDG) [3–5] for enabling precision soft-landing on planetary surfaces, which is a key component of many space missions, e.g., SLIM lander [6] on Moon and Mars Science Laboratory's Curiosity rover [7] on Mars.

The PDG problem poses many challenging demands on the vehicle in the form of safety, operational, and performance constraints, which optimization-based methods are well suited to handle. An increasingly important constraint for PDG is passive safety [8], i.e., in the event of abrupt loss of actuation, the ballistic trajectory of the vehicle must not collide with critical infrastructure near the landing site, e.g., the tower that catches the SpaceX Starship vehicle [9]. Furthermore, generating guidance trajectories with guaranteed passive safety can also lower the chances of losing the vehicle [10]. Sudden loss of actuation during powered descent, i.e., due to loss of engine thrust, is a realistic failure mode [11]. For instance, liquid rocket engines shut off if the throttle level is too low, and more recently, the SLIM lander's engine structurally failed moments before touchdown [12].

In order to handle advanced constraints such as passive safety, trajectory optimization is necessary. Trajectory optimization for PDG typically involves solving a constrained optimal control problem (OCP). Direct methods are a popular choice for solving OCPs because they are less sensitive to initialization than indirect methods and offer the flexibility to impose various path constraints on the state and input [13, Sec. 4.3]. However, direct methods can only impose constraints at finitely-many discrete time nodes, leading to potential constraint violation between the time nodes (also referred to as inter-sample constraint violation [14]). Thus, computationally expensive mesh-refinement heuristics are necessary to curtail these violations [13, Sec. 4.7].

Besides the potential inter-sample violations, imposing the passive-safety constraint in a direct method poses an additional challenge. The ballistic trajectory corresponding to each time node on the vehicle's nominal trajectory needs to be parameterized on a grid spanning a safety duration. Thus, the number of constraints in the optimization problem is a factor of the discretization grid size, making mesh-refinement more expensive [15].

In this work, we solve the fuel-optimal passively-safe PDG problem for a six-degree-of-freedom (6-DoF) lander via the recently-introduced direct method, CT-SCVX [16], which addresses the aforementioned shortcomings of the existing direct methods. The proposed approach leverages an isoperimetric reformulation [17] of the passive-safety constraint. Thus, the fidelity of satisfying the passive-safety constraint becomes independent of the discretization grid size. We can ensure continuous-time constraint satisfaction on coarse discretization grids without the need for mesh refinement. Moreover, our work represents a tractable continuous-time generalization of the discrete-time framework for passively-safe guidance presented in [15]. It also adds to recent advancements in 6-DoF PDG via sequential convex programming, particularly in the modeling of advanced constraints (e.g., due to perception [18], logical specifications [5, 19, 20], multi-phase dynamics [21], dual quaternion parametrization [22, 23], and abort safety [24]).

This paper is organized as follows. Section II describes the problem formulation and the optimal control problem in continuous time. Section III describes the CT-SCVX-based solution approach. Section IV provides a numerical demonstration of the proposed approach on a realistic lunar-landing case study. Finally, Section V provides concluding remarks.

II. Problem Statement

We consider the problem of powered-descent of a 6-DoF lander on the Moon while minimizing fuel consumption and satisfying passive-safety and path constraints. We adopt the vehicle model and the underlying assumptions from [5, Sec. II]. We assume a planetary-surface-fixed up-east-north inertial frame where the origin coincides with the landing site, and a vehicle-body-fixed frame (or simply body frame) where the origin coincides with the center of mass, the first coordinate is along the vertical body-axis, the second coordinate is along an axis that points laterally out of the vehicle, and the third coordinate is along an axis that completes the right-handed system. Further, we assume that the gravitational acceleration is constant throughout the powered-descent maneuver.

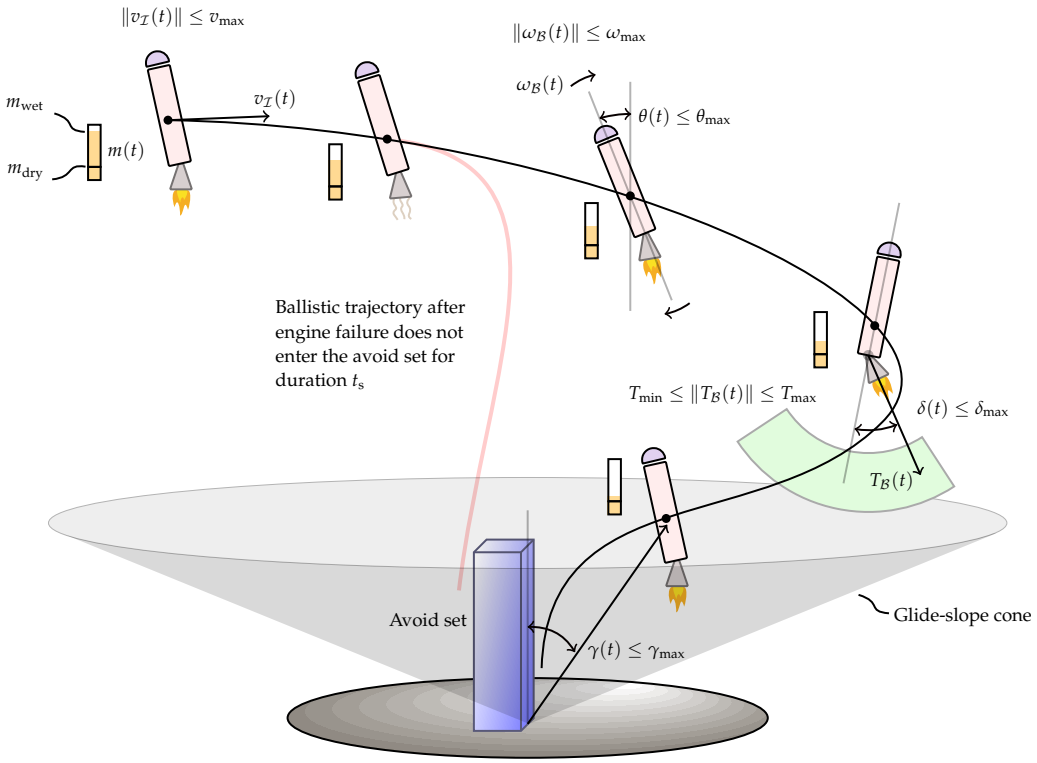

Fig. 1 Powered descent of a 6-DoF lander with path constraints (mass lower bound, position in glide-slope cone, speed upper bound, body-axis tilt-angle upper bound, angular speed upper bound, engine gimbal-angle upper bound, thrust magnitude upper and lower bound) and a passive-safety constraint with respect to the avoid set (shown in blue).

A. Dynamical Model

The dynamics the 6-DoF lander over a time interval $[t_i, t_f]$, referred to as the *planning horizon*, is governed by the following nonlinear ordinary differential equation:

$$\dot{x}(t) = f(t, x(t), u(t)), \quad t \in [t_i, t_f], \tag{1}$$

where $\dot{\square}(t) \triangleq \nabla\square(t)$, the state $x(t) \triangleq (m(t), r_{\mathcal{I}}(t), v_{\mathcal{I}}(t), q_{\mathcal{B}\leftarrow\mathcal{I}}(t), \omega_{\mathcal{B}}(t)) \in \mathbb{R}^{n_x}$ consists of vehicle mass $m(t) \in \mathbb{R}$, inertial-frame position $r_{\mathcal{I}}(t) \in \mathbb{R}^3$, inertial-frame velocity $v_{\mathcal{I}}(t) \in \mathbb{R}^3$, unit quaternion $q_{\mathcal{B}\leftarrow\mathcal{I}}(t) \in \mathbb{R}^4$ for parametrizing the transformation from the inertial to body frame, and the body-frame angular velocity $\omega_{\mathcal{B}}(t) \in \mathbb{R}^3$. The control input $u(t) \in \mathbb{R}^{n_u}$ is the body-frame thrust $T_{\mathcal{B}}(t) \in \mathbb{R}^3$ resulting from a gimbaled rocket engine.

The right-hand-side of (1) is given by:

$$f(t, x(t), u(t)) \triangleq \begin{bmatrix} -\breve{\alpha}\|T_{\mathcal{B}}(t)\| \\ v_{\mathcal{I}}(t) \\ \dfrac{1}{m(t)} C_{\mathcal{I}\leftarrow\mathcal{B}}(t) T_{\mathcal{B}}(t) + g_{\mathcal{I}} \\ \dfrac{1}{2}\Omega(\omega_{\mathcal{B}}(t)) q_{\mathcal{B}\leftarrow\mathcal{I}}(t) \\ J_{\mathcal{B}}^{-1}\left(r_{T_{\mathcal{B}}} \times T_{\mathcal{B}}(t) - \omega_{\mathcal{B}}(t) \times J_{\mathcal{B}}\omega_{\mathcal{B}}(t)\right) \end{bmatrix}, \tag{2}$$

where $\breve{\alpha}$ is the mass-depletion rate determined by the specific impulse of the rocket engine, $C_{\mathcal{I}\leftarrow\mathcal{B}}(t)$ is the direction cosine matrix corresponding to $q_{\mathcal{B}\leftarrow\mathcal{I}}(t)$, $g_{\mathcal{I}}$ is the constant inertial-frame gravitational acceleration, $\Omega(\omega_{\mathcal{B}}(t))$ is a skew-symmetric matrix [25, Eq. 5.42], $J_{\mathcal{B}}$ is the constant body-fixed inertia matrix of the vehicle

about its center of mass, and $r_{T_\mathcal{B}}$ is the body-frame moment arm formed by the engine gimbal pivot point with respect to the vehicle center of mass. Function f is continuously-differentiable except at points where the thrust magnitude is zero. However, such points will not be encountered in the proposed optimization-based method due to the thrust lower-bound constraint introduced subsequently.

While the vehicle model considered in the right-hand-side of (2) does not have an explicit time dependence, the proposed framework can handle general time-varying nonlinear systems, as shown in (1). As a result, the proposed framework allows higher fidelity vehicle models (e.g., with higher-order gravitational effects and time variation in center of mass position and inertia matrix [26, Sec. II]).

B. Path Constraints

The vehicle state and control input are subject to the following path constraints: 1) lower-bound m_{dry} on vehicle mass, 2) conic glide-slope constraint on inertial-frame position, 3) upper-bound $v_{\max}$ on vehicle speed, 4) upper-bound $\theta_{\max}$ on body-axis tilt angle, 5) upper-bound $\omega_{\max}$ on angular speed, 6) upper-bound $\delta_{\max}$ on engine gimbal angle, 7) upper-bound $T_{\max}$ on thrust magnitude, and 8) lower-bound $T_{\min}$ on thrust magnitude. Then the path constraints can be represented as:

$$g(t,x(t),u(t)) \triangleq \begin{bmatrix} m_{\text{dry}} - m(t) \\ \|\cot\gamma_{\max} H_\gamma r_\mathcal{I}(t)\|_2^2 - (r_\mathcal{I}(t)^\top e_1^3)^2 \\ -r_\mathcal{I}(t)^\top e_1^3 \\ \|v_\mathcal{I}(t)\|^2 - v_{\max}^2 \\ \|2H_\theta q_{\mathcal{B}\leftarrow\mathcal{I}}(t)\|^2 - (\cos\theta_{\max} - 1)^2 \\ \|\omega_\mathcal{B}(t)\|^2 - \omega_{\max}^2 \\ \|\cos\delta_{\max} T_\mathcal{B}(t)\|^2 - (T_\mathcal{B}(t)^\top e_1^3) \\ -T_\mathcal{B}(t)^\top e_1^3 \\ \|T_\mathcal{B}(t)\|^2 - T_{\max}^2 \\ T_{\min}^2 - \|T_\mathcal{B}(t)\|^2 \end{bmatrix} \leq 0_{n_g}, \tag{3}$$

where $n_g = 10$, $H_\gamma = \begin{bmatrix} e_2^3 & e_3^3 \end{bmatrix}^\top$, and $H_\theta = \begin{bmatrix} e_2^4 & e_3^4 \end{bmatrix}^\top$ (if scalar-last convention is used for quaternions). The body-axis tilt angle is $\theta(t) \triangleq \arccos\left(1 - 2\|H_\theta q_{\mathcal{B}\leftarrow\mathcal{I}}(t)\|\right)$, the angle between the inertial-frame position vector and the axis of the glide-slope cone is $\gamma(t) \triangleq \arctan\left(\|H_\gamma r_\mathcal{I}(t)\| / r_\mathcal{I}(t)^\top e_1^3\right)$, and the angle between the body-frame thrust vector and the body-axis is $\delta(t) \triangleq \arccos\left(T_\mathcal{B}(t)^\top e_1^3 / \|T_\mathcal{B}(t)\|\right)$. Figure 1 illustrates the path constraints in (3). Despite the absence of time-variation in the right-hand-side of (3), we include a time argument for g to ensure generality of the proposed framework.

We require g to be a continuously-differentiable function. To that end, the glide-slope and gimbal-angle constraints, which are originally second-order-cone constraints, are equivalently represented as a combination of quadratic and linear inequalities [27, Sec. 3.2.4] as follows:

$$\|\cot\gamma_{\max} H_\gamma r_\mathcal{I}(t)\| \leq r_\mathcal{I}(t)^\top e_1^3 \iff \|\cot\gamma_{\max} H_\gamma r_\mathcal{I}(t)\|^2 \leq (r_\mathcal{I}(t)^\top e_1^3)^2,\ \ r_\mathcal{I}(t)^\top e_1^3 \geq 0, \tag{4a}$$

$$\|\cos\delta_{\max} T_\mathcal{B}(t)\| \leq T_\mathcal{B}(t)^\top e_1^3 \iff \|\cos\delta_{\max} T_\mathcal{B}(t)\|^2 \leq (T_\mathcal{B}(t)^\top e_1^3)^2,\ \ T_\mathcal{B}(t)^\top e_1^3 \geq 0. \tag{4b}$$

C. Passive-Safety Constraint

We require the vehicle's trajectory to be passively safe with respect to an avoid set $\mathcal{A} \triangleq \{z \in \mathbb{R}^{n_x} \mid Az < b\}$ for duration t_s, where $A = [a_1 \ \dots \ a_m]^\top$ and $b = (b_1, \dots, b_m)$, with $a_i \in \mathbb{R}^{n_x}$ and $b_i \in \mathbb{R}$ for $i = 1, \dots, m$. Passive-safety is determined by the ballistic trajectory of the vehicle (i.e., without control inputs). Given $\gamma > 0$ and $t \in [t_i, t_f]$, the ballistic trajectory over $[t, t+\gamma]$ starting from $x(t)$ is defined as:

$$F_{\text{fd}}(t, x(t), \gamma) \triangleq x(t) + \int_0^\gamma f(\theta + t, \xi(\theta), 0_{n_u}) \mathrm{d}\theta, \tag{5}$$

where $\xi(\theta)$ satisfies the initial value problem (IVP):

$$\nabla\xi(\theta) = f(\theta + t, \xi(\theta), 0_{n_u}), \quad \theta \in [0, \gamma], \tag{6a}$$
$$\xi(0) = x(t). \tag{6b}$$

Then the passive-safety constraint is:

$$F_{\text{fd}}(t, x(t), \gamma) \notin \mathcal{A}, \quad \forall\, \gamma \in [0, t_{\text{s}}],\ \forall\, t \in [t_{\text{i}}, t_{\text{f}}]. \tag{7}$$

We refer to the time interval $[0, t_{\text{s}}]$ as the *safety horizon*.

D. Optimal Control Problem

The free-final-time optimal control problem for passively-safe fuel-optimal powered descent of the 6-DoF lander can be stated in continuous-time as:

$$\underset{t_{\text{f}},\, x(t),\, u(t)}{\text{minimize}} \quad -x(t_{\text{f}})^{\top} e_1^{n_x}, \tag{8a}$$
$$\text{subject to} \quad \dot{x}(t) = f(t, x(t), u(t)), \qquad t \in [t_{\text{i}}, t_{\text{f}}], \tag{8b}$$
$$g(t, x(t), u(t)) \leq 0, \qquad t \in [t_{\text{i}}, t_{\text{f}}], \tag{8c}$$
$$F_{\text{fd}}(t, x(t), \gamma) \notin \mathcal{A}, \qquad \gamma \in [0, t_{\text{s}}],\ t \in [t_{\text{i}}, t_{\text{f}}], \tag{8d}$$
$$P(t_{\text{i}}, x(t_{\text{i}}), t_{\text{f}}, x(t_{\text{f}})) = 0. \tag{8e}$$

The boundary conditions at the initial and final times are encoded as a (potentially nonlinear) equality constraint (8e), where t_{f} is a decision variable and t_{i} is a constant.

III. CT-SCvx Solution Approach

This section describes a solution approach for (8) based on the recently-introduced CT-SCvx framework [16] which combines several key methods: 1) isoperimetric reformulation of path and passive-safety constraints, 2) time-dilation for handling free-final-time problems, 3) multiple-shooting discretization, 4) ℓ_1-exact penalization or nonconvex constraints, and 5) the prox-linear method [28], which is a convergence-guaranteed sequential convex programming (SCP) algorithm for convex-composite minimization.

A. Isoperimetric Constraint Reformulation & Time-Dilation

Imposing path and passive-safety constraints at discrete time instants, as is common in most direct methods [29, Fig. 34], inevitably leads to inter-sample constraint violations. Alternatively, we can relate the pointwise satisfaction of these constraints to their cumulative violation over the planning horizon, measured with a continuously-differentiable exterior penalty function. Constraining the cumulative violation to zero is equivalent to imposing the constraints pointwise within the planning horizon.

More precisely, the pointwise satisfaction of the path constraint can be equated to the cumulative violation of the path constraint over the planning horizon as follows:

$$\int_0^{t_{\text{f}}} \|g(t, x(t), u(t))\|_+^2 \,\mathrm{d}t = 0 \iff g(t, x(t), u(t)) \leq 0_{n_g}, \quad \forall\, t \in [t_{\text{i}}, t_{\text{f}}], \tag{9}$$

where the integral equation on the left is called the *isoperimetric form* of the path constraint [17, Eq. 6]. Note that the exterior penalty function, $\square \mapsto |\square|_+^2$, is continuously differentiable.

The passive-safety constraint can be subjected to a similar transformation. First, constraint (7) is equivalently stated in terms of signed distance to $\mathcal{A}$ as follows:

$$\text{sdist}_{\mathcal{A}}(F_{\text{fd}}(t, x(t), \gamma)) \geq 0 \iff F_{\text{fd}}(t, x(t), \gamma) \notin \mathcal{A}. \tag{10}$$

Since numerical optimization methods cannot directly handle strict inequalities, we chose $\mathcal{A}$ to be an open set in Section II.C. As a result, the left-hand-side of (10) is a non-strict inequality. Next, we define the cumulative

violation of the passive-safety constraint at time t as:

$$\Gamma(t, x(t)) \triangleq \int_0^{t_s} |-\mathrm{sdist}_{\mathcal{A}}(F_{\mathrm{fd}}(t, x(t), \gamma))|_+^2 \mathrm{d}\gamma. \tag{11}$$

Then we obtain:

$$\Gamma(t, x(t)) = 0, \quad \forall t \in [t_i, t_f] \iff F_{\mathrm{fd}}(t, x(t), \gamma) \notin \mathcal{A}, \quad \forall\, \gamma \in [0, t_s], \forall\, t \in [t_i, t_f]. \tag{12}$$

We can solve the IVP:

$$\begin{aligned}
\nabla \xi(\gamma) &= f(\gamma + t, \xi(\gamma), 0_{n_u}), && \gamma \in [0, t_s], && \text{(13a)}\\
\nabla \zeta(\gamma) &= |-\mathrm{sdist}_{\mathcal{A}}(\xi(\gamma))|_+^2, && \gamma \in [0, t_s], && \text{(13b)}\\
\xi(0) &= x(t), && && \text{(13c)}\\
\zeta(0) &= 0, && && \text{(13d)}
\end{aligned}$$

to obtain $\Gamma(t, x(t)) = \zeta(t_s)$.

Finally, we augment the chaser's dynamical system with a new state to measure the cumulative violations of the path and passive-safety constraints across the planning horizon.

$$\begin{aligned}
\dot{x}(t) &= f(t, x(t), u(t)), && t \in [t_i, t_f], && \text{(14a)}\\
\dot{y}(t) &= \begin{bmatrix} \|g(t, x(t), u(t))\|_+^2 \\ \Gamma(t, x(t)) \end{bmatrix}, && t \in [t_i, t_f]. && \text{(14b)}
\end{aligned}$$

Observe that imposing the periodic boundary condition, $y(0) = y(t_f)$, ensures that $g(t, x(t), u(t)) \leq 0_{n_g}$ and $\Gamma(t, x(t)) = 0$ hold for all $t \in [t_i, t_f]$.

We adopt the time-dilation approach [30, Eq. 4.5], [16, Sec. 2.4] to transform (8) into a fixed-final-time optimal control problem. Let the actual time t (within the planning horizon) be a strictly increasing, smooth function of $\tau \in [0, 1]$, such that $t(0) = t_i$ and $t(1) = t_f$. Let the derivative of this function (called the *dilation factor*) be denoted by $s(\tau)$ for $\tau \in [0, 1]$. Then we have:

$$\begin{aligned}
\overset{\circ}{x}(\tau) &= s(\tau) f(t(\tau), x(\tau), u(\tau)), && \tau \in [0, 1], && \text{(15a)}\\
\overset{\circ}{y}(\tau) &= s(\tau) \begin{bmatrix} \|g(t(\tau), x(\tau), u(\tau))\|_+^2 \\ \Gamma(t(\tau), x(\tau)) \end{bmatrix}, && \tau \in [0, 1], && \text{(15b)}\\
\overset{\circ}{t}(\tau) &= s(\tau), && \tau \in [0, 1], && \text{(15c)}
\end{aligned}$$

where $\overset{\circ}{\square}(\tau) \triangleq \nabla \square(\tau)$. Due to the strict monotonicity of $t(\tau)$, we treat τ as the new independent variable (i.e., we have replaced $\square(t(\tau))$ with $\square(\tau)$, where $\square \in \{x, y, u\}$). We define an augmented state: $\tilde{x}(\tau) \triangleq (x(\tau), y(\tau), t(\tau))$, and an augmented control input: $\tilde{u}(\tau) \triangleq (u(\tau), s(\tau))$. Then the augmented dynamical system can be compactly represented as:

$$\overset{\circ}{\tilde{x}}(\tau) = \tilde{f}(\tilde{x}(\tau), \tilde{u}(\tau)) \triangleq s(\tau) \begin{bmatrix} f(t(\tau), x(\tau), u(\tau)) \\ \|g(t(\tau), x(\tau), u(\tau))\|_+^2 \\ \Gamma(t(\tau), x(\tau)) \\ 1 \end{bmatrix}, \quad \tau \in [0, 1]. \tag{16}$$

Note that $\tilde{f}$ is almost-everywhere continuously differentiable. We define $n_{\tilde{x}} \triangleq n_x + 3$ after augmenting x with y and t, $n_{\tilde{u}} \triangleq n_u + 1$ after augmenting u with s, and a *selector matrix* ${}^{\square}E$ to select $\square$ from $\tilde{x}$: $\square = {}^{\square}E\tilde{x}$ for $\square \in \{x, y, t\}$. Similarly, $\square = {}^{\square}E\tilde{u}$ for $\square \in \{u, s\}$.

B. Discretized Nonconvex Problem

We use a zero-order-hold parametrization* for the augmented control input to discretize (16) over a grid of size N within $[0, 1]$, denoted by $0 = \tau_1 < \ldots < \tau_N = 1$. For each $k = 1, \ldots, N-1$, we define:

$$\tilde{F}_k(\tilde{x}_k, \tilde{u}_k) \triangleq \tilde{x}_k + \int_{\tau_k}^{\tau_{k+1}} \tilde{f}(\tilde{\xi}(\tau), \tilde{u}_k) \mathrm{d}\tau, \tag{17}$$

*Other parametrizations such as first-order-hold (FOH) and pseudospectral polynomials can be readily-handled without any modifications.

where $\tilde{\xi}(\tau)$ solves the IVP:

$$\nabla\tilde{\xi}(\tau) = \tilde{f}(\tilde{\xi}(\tau), \tilde{u}_k), \quad \tau \in [\tau_k, \tau_{k+1}], \tag{18a}$$
$$\tilde{\xi}(\tau_k) = \tilde{x}_k. \tag{18b}$$

The representation in (17) is commonly referred to as multiple-shooting discretization [31] and is equivalent to the differential form in (16). Then the discretized augmented dynamics constraint is:

$$\tilde{x}_{k+1} = \tilde{F}_k(\tilde{x}_k, \tilde{u}_k), \quad k = 1, \ldots, N-1. \tag{19}$$

After applying the isoperimetric reformulation, the time-dilation, and the multiple-shooting discretization with zero-order-hold parametrization, the optimal control problem in (8) transforms into the finite-dimensional nonconvex optimization problem:

$$\underset{\tilde{x}_k, \tilde{u}_k}{\text{minimize}} \quad -\tilde{x}_N^\top e_1^{n_{\tilde{x}}}, \tag{20a}$$
$$\text{subject to} \quad \tilde{x}_{k+1} = \tilde{F}_k(\tilde{x}_k, \tilde{u}_k), \qquad k = 1, \ldots, N-1, \tag{20b}$$
$${}^{y}E\tilde{x}_{k+1} = {}^{y}E\tilde{x}_k, \tag{20c}$$
$${}^{t}E\tilde{x}_1 = t_\mathrm{i}, \tag{20d}$$
$$P({}^{t}E\tilde{x}_1, {}^{x}E\tilde{x}_1, {}^{t}E\tilde{x}_N, {}^{x}E\tilde{x}_N) = 0. \tag{20e}$$

The satisfaction of constraints (20b) and (20c) ensure dynamic feasibility, i.e., the satisfaction of (1), and continuous-time feasibility of path constraints (3) and passive-safety constraint (7). In practice, we relax (20c) into:

$${}^{y}E(\tilde{x}_{k+1} - \tilde{x}_k) \leq \epsilon 1_2, \quad k = 1, \ldots, N-1, \tag{21}$$

where ϵ is a small positive constant, to ensure that constraint qualification holds for (20) and to enable exact penalization, see [16, Sec. 3.1] for a detailed discussion. Furthermore, for a given ϵ, we can estimate the maximum pointwise violation of the path and passive-safety constraints, see [16, Sec. 3.3]. In practice, we observe that even numerically significant values for ϵ, e.g., $\epsilon = 10^{-4}$, can yield physically insignificant pointwise violation of the constraints.

Next we subject (20b) (and (20e) if P is nonlinear) to ℓ_1 penalization, along with the relaxation of (20c), to obtain a penalized problem with a closed, convex feasible set. We use the prox-linear method, an SCP algorithm which is guaranteed to find a stationary point for the penalized problem. If such a stationary point is feasible, then it is guaranteed to be a Karush-Kuhn-Tucker (KKT) point of (20) (with the relaxation for (20c)). We refer the reader to [16, Sec. 4] for further discussion about the convergence guarantees. Appendix A describes the linearization of (20b), which is a key step within CT-SCvx.

In a practical implementation, scaling of the decision variables and constraints, and tuning of the ℓ_1 penalty parameter play a key role in ensuring reliable numerical performance of the solution method, see the discussion in [29, p. 78]. Furthermore, the consolidation of the state and control input constraints into a dynamical system, i.e., the augmented system, simplifies the implementation of a customized CT-SCvx-based solver for (20), as demonstrated in [32].

IV. Numerical Results

We demonstrate the proposed CT-SCvx-based framework for passively-safe fuel-optimal powered descent on a lunar-landing case study. Table 1 shows the parameter values chosen for the problem. The boundary conditions constraint function P is chosen to impose: 1) initial condition: mass (m_wet), position (r_i), velocity (v_i), angular velocity (0_3), 2) final condition: position (r_f), velocity (v_f), quaternion (q_id), angular velocity (0_3), and 3) upper-bound on final time ($t_{\mathrm{f,\,max}}$).

Figure 2 compares the position trajectories of safe powered-descent maneuver from the proposed approach and the baseline maneuver without the passive-safety constraint. The continuous-time profiles of speed, angular speed, and thrust magnitude for the safe maneuver shown in Figure 3 satisfy the constraints (dashed red lines) at all times. The body-axis orientation (red line) and the thrust vector (green line) shown in Figure

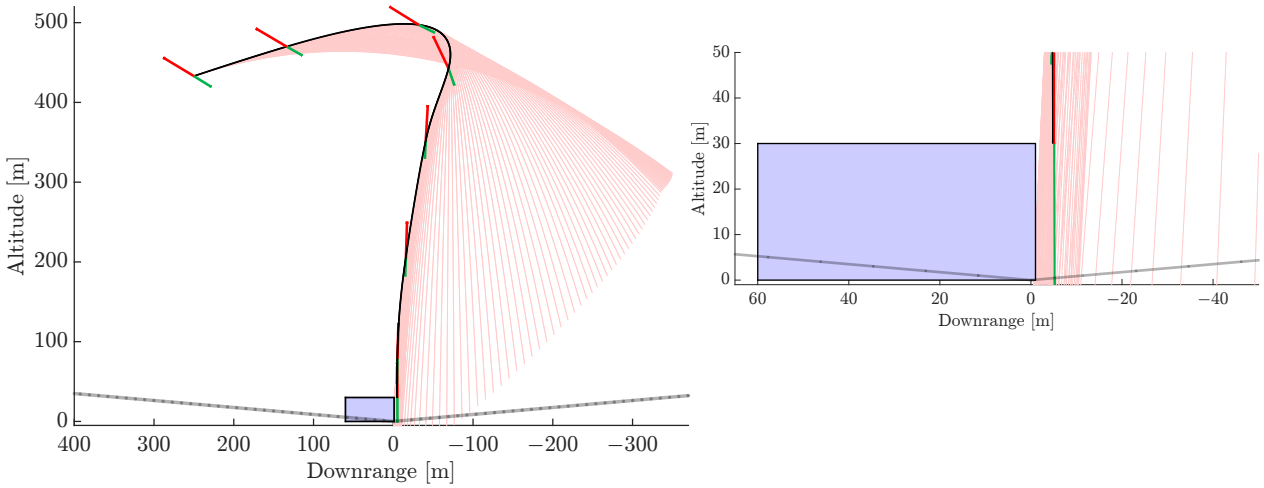

(a) Safe trajectory

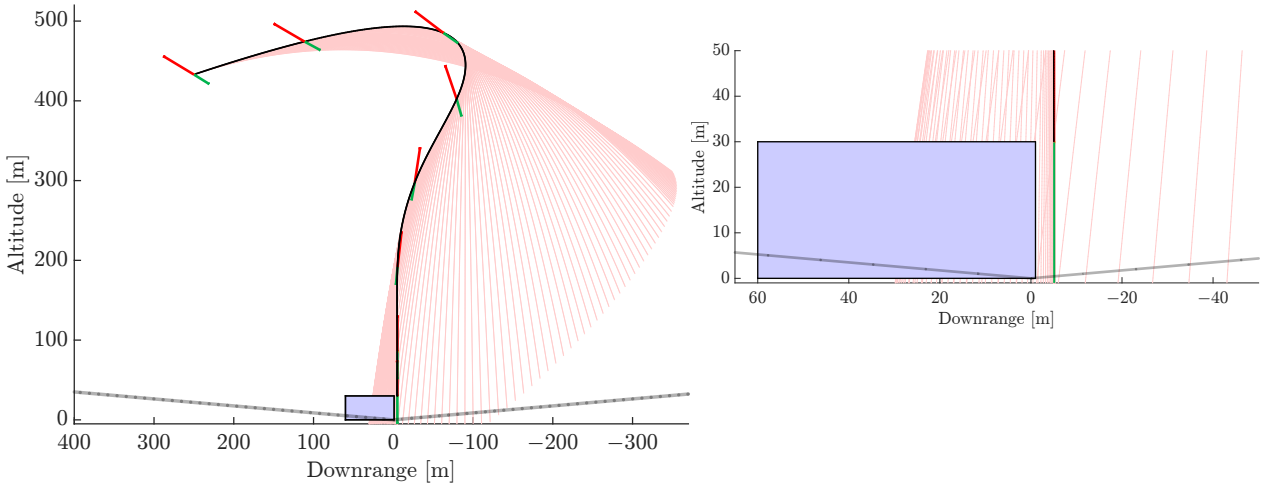

(b) Unsafe trajectory

Fig. 2 The powered-descent maneuver shown in (a) is passively-safe with respect to the avoid set (blue-box) for $t_s = 20$ s, while the baseline maneuver in (b) is unsafe since it is generated without the passive-safety constraint. Altitude is along the third coordinate and downrange is along the second coordinate of the inertial-frame coordinate axes. The light red curves denote the ballistic trajectories after engine failure (shutdown), the red lines indicate the body-axis orientation, and the green lines indicate the thrust vector.

2, and the black dots shown in Figure 3, correspond to the discretization nodes of CT-SCVX. The black curves correspond to the continuous-time evolution of (1) over the planning horizon using the computed control input solution.

Observe that the ballistic trajectories (light red curves) corresponding to the safe maneuver in Figure 2a are concentrated just outside the avoid-set (to the right side). Such a maneuver ensures safety without sacrificing on fuel efficiency: the safe maneuver only consumes 12 kg more fuel than the (unsafe) baseline maneuver, which is less than 0.5% of m_{wet}.

The evaluation of the partial derivatives of $\tilde{f}$, shown in Appendix A, involves solving a 240-dimensional IVP (29). Therefore, the computation of the second derivatives of $\tilde{f}$ (if they exist) would involve an IVP with dimensions more than 38000, which would dramatically increase the computation cost. Thus, it would be prohibitively expensive to solve (20) using an IPM- or SQP-based solver that requires Hessian information, compared to the proposed CT-SCVX-based approach that only requires gradient information.

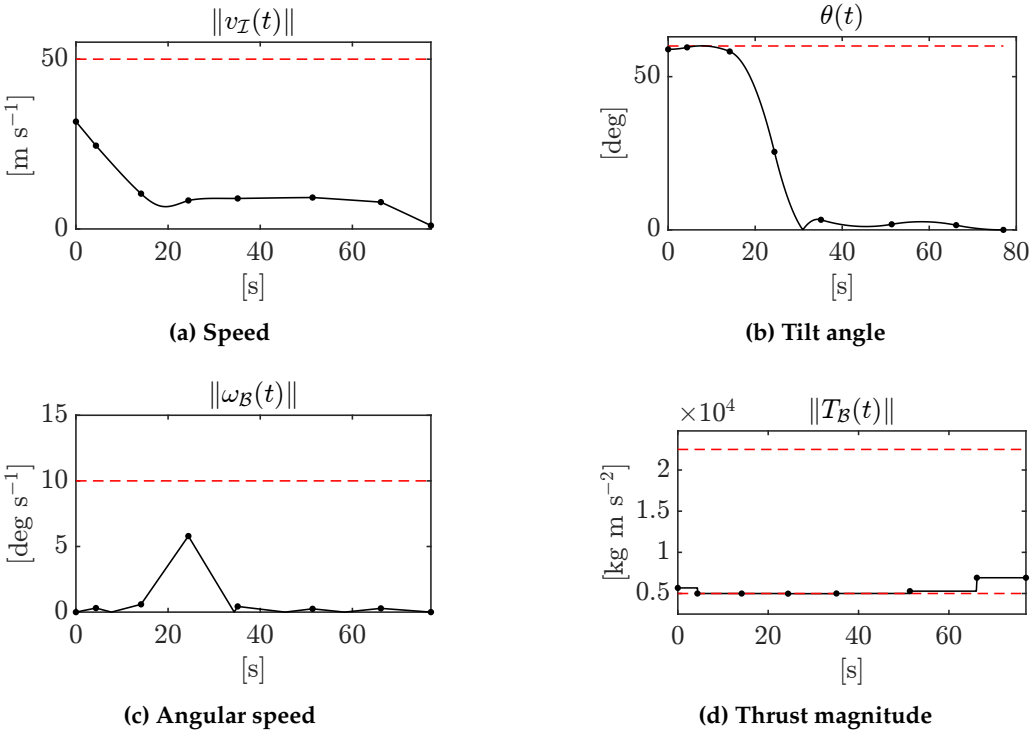

(a) Speed **(b) Tilt angle**

(c) Angular speed **(d) Thrust magnitude**

Fig. 3 The continuous-time profiles of speed, tilt angle, angular speed, and thrust magnitude for the passively-safe powered-descent maneuver. Constraint bounds are shown as red dashed lines.

Table 1 Parameter values for problem (20)

Parameter	Value
$\check{\alpha}$	4.53×10^{-4} s m^{-1}
$g_{\mathcal{I}}$	$(-1.61, 0, 0)$ m s^{-2}
$r_{T_{\mathcal{B}}}$	$(-0.25, 0, 0)$ m
$J_{\mathcal{B}}$	$\mathrm{diag}(19150, 13600, 13600)$ kg m^2
$t_{\mathrm{i}}, t_{\mathrm{f,max}}$	0, 90 s
$m_{\mathrm{dry}}, m_{\mathrm{wet}}$	2100, 3250 kg
$r_{\mathrm{i}}, r_{\mathrm{f}}$	$(433, 0, 250)$, $(30, 0, -5)$ m
$v_{\mathrm{i}}, v_{\mathrm{f}}$	$(10, 0, -30)$, $(-1, 0, 0)$ m s^{-1}
q_{id}	unit quaternion
γ_{max}	85°
v_{max}	50 m s^{-1}
θ_{max}	60°
ω_{max}	10° s^{-1}
δ_{max}	45°
$T_{\mathrm{min}}, T_{\mathrm{max}}$	5000, 22000 N
$\mathcal{A}$	$\{z \in \mathbb{R}^{n_x} \mid Az < b\}$, $A = \begin{bmatrix} 0_6 & \begin{bmatrix} I_3 \\ -I_3 \end{bmatrix} & 0_{6\times 10} \end{bmatrix}$, $b = (30, 30, 60, 0, 30, 1)$
ϵ	10^{-4}
N	8

V. Conclusion

We developed an optimization-based solution method for the fuel-optimal powered descent of a six-degree-of-freedom (6-DoF) lander, which ensures passive safety with respect to an avoid-set near the landing site for a specified time horizon. This method guarantees that the vehicle's ballistic trajectory, in the event of unplanned engine shutdown, does not enter an avoid set containing critical infrastructure within the specified duration. These safety constraints must be satisfied in continuous time. Imposing them at finitely-many time nodes, as is common in most direct methods, can cause inter-sample constraint violations. To address this, the proposed approach leveraged the recently introduced CT-SCVX framework, wherein the set-based passive-safety constraint was subjected to an isoperimetric reformulation to ensure continuous-time constraint satisfaction. We provided a numerical demonstration of the proposed approach using a realistic lunar-landing case study.

A. Linearization of Discretized Augmented System

Computing linearizations of (19) is a key step within CT-SCVX, see [16, Sec. 3.2] for further details. Given reference augmented states and control inputs: $\bar{\tilde{x}}_1, \ldots, \bar{\tilde{x}}_N$, $\bar{\tilde{u}}_1, \ldots, \bar{\tilde{u}}_{N-1}$, a linear approximation for constraint (19) is given by the first-order Taylor expansion of $\tilde{F}_k$:

$$\begin{aligned} \tilde{x}_{k+1} &= \tilde{F}_k(\bar{\tilde{x}}_k, \bar{\tilde{u}}_k) + \nabla_1 \tilde{F}_k(\bar{\tilde{x}}_k, \bar{\tilde{u}}_k)(\tilde{x}_k - \bar{\tilde{x}}_k) + \nabla_2 \tilde{F}_k(\bar{\tilde{x}}_k, \bar{\tilde{u}}_k)(\tilde{u}_k - \bar{\tilde{u}}_k), && (22)\\ &= \tilde{A}_k \tilde{x}_k + \tilde{B}_k \tilde{u}_k + \tilde{c}_k, && (23) \end{aligned}$$

where:

$$\begin{aligned} \tilde{A}_k &\triangleq \nabla_1 \tilde{F}_k(\bar{\tilde{x}}_k, \bar{\tilde{u}}_k), && (24a)\\ \tilde{B}_k &\triangleq \nabla_2 \tilde{F}_k(\bar{\tilde{x}}_k, \bar{\tilde{u}}_k), && (24b)\\ \tilde{c}_k &\triangleq \tilde{F}(\bar{\tilde{x}}_k, \bar{\tilde{u}}_k) - \tilde{A}_k \bar{\tilde{x}}_k - \tilde{B}_k \bar{\tilde{u}}_k. && (24c) \end{aligned}$$

Next we evaluate the partial derivatives of $\tilde{F}_k$ at $\bar{\tilde{x}}_k$, $\bar{\tilde{u}}_k$:

$$\begin{aligned} \tilde{A}_k &= I_{n_{\tilde{x}}} + \int_{\tau_k}^{\tau_{k+1}} \nabla_1 \tilde{f}(\tilde{\xi}(\tau), \bar{\tilde{u}}_k)\tilde{\Phi}(\tau)\mathrm{d}\tau, && (25a)\\ \tilde{B}_k &= \int_{\tau_k}^{\tau_{k+1}} \nabla_1 \tilde{f}(\tilde{\xi}(\tau), \bar{\tilde{u}}_k)\tilde{\Psi}(\tau) + \nabla_2 \tilde{f}(\tilde{\xi}(\tau), \bar{\tilde{u}}_k)\mathrm{d}\tau. && (25b) \end{aligned}$$

Equivalently, the solution to the IVP:

$$\begin{aligned} \nabla\tilde{\xi}(\tau) &= \tilde{f}(\tilde{\xi}(\tau), \tilde{u}_k), && \tau \in [\tau_k, \tau_{k+1}], && (26a)\\ \nabla\tilde{\Phi}(\tau) &= \nabla_1 \tilde{f}(\tilde{\xi}(\tau), \bar{\tilde{u}}_k)\tilde{\Phi}(\tau), && \tau \in [\tau_k, \tau_{k+1}], && (26b)\\ \nabla\tilde{\Psi}(\tau) &= \nabla_1 \tilde{f}(\tilde{\xi}(\tau), \bar{\tilde{u}}_k)\tilde{\Psi}(\tau) + \nabla_2 \tilde{f}(\tilde{\xi}(\tau), \bar{\tilde{u}}_k), && \tau \in [\tau_k, \tau_{k+1}], && (26c)\\ \tilde{\xi}(\tau_k) &= \bar{\tilde{x}}_k, && && (26d)\\ \tilde{\Phi}(\tau_k) &= I_{n_{\tilde{x}}}, && && (26e)\\ \tilde{\Psi}(\tau_k) &= 0_{n_{\tilde{x}} \times n_{\tilde{u}}}, && && (26f) \end{aligned}$$

provides $\tilde{A}_k = \tilde{\Phi}(\tau_{k+1})$ and $\tilde{B}_k = \tilde{\Psi}(\tau_{k+1})$.

A key step in solving (26) is the computation of the partial derivatives of $\tilde{f}$. Given $\tilde{x} = (x, y, t)$ and $\tilde{u} = (u, s)$,

the partial derivatives of $\tilde{f}$ are:

$$\nabla_1 \tilde{f}(\tilde{x},\tilde{u}) = s\begin{bmatrix} \nabla_2 f(t,x,u) & 0_{n_x\times 2} & \nabla_1 f(t,x,u) \\ 2|g(t,x,u)|_+^\top \nabla_2 g(t,x,u) & 0_2^\top & 2|g(t,x,u)|_+^\top \nabla_1 g(t,x,u) \\ \nabla_2 \Gamma(t,x) & 0_2^\top & \nabla_1 \Gamma(t,x) \\ 0_{n_x}^\top & 0_2^\top & 0 \end{bmatrix}, \tag{27a}$$

$$\nabla_2 \tilde{f}(\tilde{x},\tilde{u}) = \begin{bmatrix} s\nabla_3 f(t,x,u) & f(t,x,u) \\ 2s|g(t,x,u)|_+^\top \nabla_3 g(t,x,u) & \|g(t,x,u)\|_+^2 \\ 0_{n_u}^\top & \Gamma(t,x) \\ 0_{n_u}^\top & 1 \end{bmatrix}, \tag{27b}$$

$$= \begin{bmatrix} s\begin{bmatrix} \nabla_3 f(t,x,u) \\ 2|g(t,x,u)|_+^\top \nabla_3 g(t,x,u) \\ 0_{n_u}^\top \\ 0_{n_u}^\top \end{bmatrix} \frac{1}{s}\tilde{f}(\tilde{x},\tilde{u}) \end{bmatrix}, \tag{27c}$$

where the partial derivatives of Γ and F_{fd} are given by:

$$\nabla_i \Gamma(t,x) = -2\int_0^{t_s} |-\text{sdist}_{\mathcal{A}}(F_{\text{fd}}(t,x,\gamma))|_+ \nabla \text{sdist}_{\mathcal{A}}(F_{\text{fd}}(t,x,\gamma)) \nabla_i F_{\text{fd}}(t,x,\gamma) \text{d}\gamma, \quad i=1,2, \tag{28a}$$

$$\nabla_1 F_{\text{fd}}(t,x,\gamma) = \int_0^\gamma \nabla_1 f(\theta+t,\xi(\theta),0_{n_u}) + \nabla_2 f(\theta+t,\xi(\theta),0_{n_u}) \frac{\partial \xi(\theta)}{\partial t} \text{d}\theta, \tag{28b}$$

$$\nabla_2 F_{\text{fd}}(t,x,\gamma) = I_{n_x} + \int_0^\gamma \nabla_2 f(\theta+t,\xi(\theta),0_{n_u}) \frac{\partial \xi(\theta)}{\partial x} \text{d}\theta. \tag{28c}$$

For notational convenience, we denote $\Phi(\theta) = \dfrac{\partial \xi(\theta)}{\partial x}$ and $\psi(\theta) = \dfrac{\partial \xi(\theta)}{\partial t}$. Then we solve the following initial value problem:

$$\begin{aligned}
\nabla \xi(\theta) &= f(\theta+t,\xi(\theta),0_{n_u}), && \theta\in[0,t_s], && (29a)\\
\nabla \zeta(\theta) &= |-\text{sdist}_{\mathcal{A}}(\xi(\theta))|_+^2, && \theta\in[0,t_s], && (29b)\\
\nabla \Phi(\theta) &= \nabla_2 f(\theta+t,\xi(\theta),0_{n_u})\Phi(\theta), && \theta\in[0,t_s], && (29c)\\
\nabla \psi(\theta) &= \nabla_2 f(\theta+t,\xi(\theta),0_{n_u})\psi(\theta) + \nabla_1 f(\theta+t,\xi(\theta),0_{n_u}), && \theta\in[0,t_s], && (29d)\\
\nabla \omega(\theta) &= -2|-\text{sdist}_{\mathcal{A}}(\xi(\theta))|_+ \Phi(\theta)^\top \nabla \text{sdist}_{\mathcal{A}}(\xi(\theta))^\top, && \theta\in[0,t_s], && (29e)\\
\nabla \lambda(\theta) &= -2|-\text{sdist}_{\mathcal{A}}(\xi(\theta))|_+ \nabla \text{sdist}_{\mathcal{A}}(\xi(\theta))\psi(\theta), && \theta\in[0,t_s], && (29f)\\
\xi(0) &= x, && && (29g)\\
\zeta(0) &= 0, && && (29h)\\
\Phi(0) &= I_{n_x}, && && (29i)\\
\psi(0) &= 0_{n_x}, && && (29j)\\
\omega(0) &= 0_{n_x}, && && (29k)\\
\lambda(0) &= 0. && && (29l)
\end{aligned}$$

to obtain:

$$\begin{aligned}
\Gamma(t,x) &= \zeta(t_s), && (30a)\\
\nabla_1 \Gamma(t,x) &= \lambda(t_s), && (30b)\\
\nabla_2 \Gamma(t,x) &= \omega(t_s)^\top. && (30c)
\end{aligned}$$

References

[1] Di Cairano, S., and Kolmanovsky, I. V., "Real-time optimization and model predictive control for aerospace and automotive applications," *2018 Annual American Control Conference (ACC)*, IEEE, 2018, pp. 2392–2409. https://doi.org/10.23919/acc.2018.8431585.

[2] Malyuta, D., Yu, Y., Elango, P., and Açıkmeşe, B., "Advances in trajectory optimization for space vehicle control," *Annual Reviews in Control*, Vol. 52, 2021, pp. 282–315. https://doi.org/10.1016/j.arcontrol.2021.04.013.

[3] Açıkmeşe, B., and Ploen, S. R., "Convex Programming Approach to Powered Descent Guidance for Mars Landing," *Journal of Guidance, Control, and Dynamics*, Vol. 30, No. 5, 2007, pp. 1353–1366. https://doi.org/10.2514/1.27553.

[4] Blackmore, L., "Autonomous precision landing of space rockets," *Frontiers of Engineering: Reports on Leading-Edge Engineering from the 2016 Symposium*, Vol. 46, The Bridge Washington, DC, 2016, pp. 15–20.

[5] Szmuk, M., Reynolds, T. P., and Açıkmeşe, B., "Successive Convexification for Real-Time Six-Degree-of-Freedom Powered Descent Guidance with State-Triggered Constraints," *Journal of Guidance, Control, and Dynamics*, Vol. 43, No. 8, 2020, pp. 1399–1413. https://doi.org/10.2514/1.G004549.

[6] Haruyama, J., Sawai, S., Mizuno, T., Yoshimitsu, T., Fukuda, S., and Nakatani, I., "Exploration of Lunar Holes, Possible Skylights of Underlying Lava Tubes, by Smart Lander for Investigating Moon (SLIM)," *Transactions of the Japan Society for Aeronautics and Space Sciences*, Vol. 10, No. ists28, 2012, pp. 7–10. https://doi.org/10.2322/tastj.10.pk_7.

[7] Grotzinger, J. P., Crisp, J., Vasavada, A. R., Anderson, R. C., Baker, C. J., Barry, R., Blake, D. F., Conrad, P., Edgett, K. S., Ferdowski, B., Gellert, R., Gilbert, J. B., Golombek, M., Gómez-Elvira, J., Hassler, D. M., Jandura, L., Litvak, M., Mahaffy, P., Maki, J., Meyer, M., Malin, M. C., Mitrofanov, I., Simmonds, J. J., Vaniman, D., Welch, R. V., and Wiens, R. C., "Mars Science Laboratory Mission and Science Investigation," *Space Science Reviews*, Vol. 170, 2012, pp. 5–56. https://doi.org/10.1007/s11214-012-9892-2.

[8] Marsillach, D. A., Di Cairano, S., and Weiss, A., "Fail-safe Rendezvous Control on Elliptic Orbits using Reachable Sets," *2020 American Control Conference (ACC)*, IEEE, 2020, p. 4920–4925. https://doi.org/10.23919/acc45564.2020.9147957.

[9] Wall, M., "SpaceX's Starship booster was '1 second away' from aborting epic launch-tower catch," , 2024. URL https://www.space.com/spacex-starship-super-heavy-chopsticks-catch-near-abort, Accessed: 2024-12-02.

[10] Wall, M., "SpaceX's Starship Soars in 6th Test Flight but Skips Booster Catch," , 2024. URL https://www.scientificamerican.com/article/spacexs-starship-soars-in-6th-test-flight-but-skips-booster-catch/, Accessed: 2024-12-02.

[11] Clark, S., "Component fatigue caused early shutdown of Merlin engine on last SpaceX launch," , 2021. URL https://spaceflightnow.com/2021/03/01/component-fatigue-caused-early-shutdown-of-merlin-engine-on-last-spacex-launch/, Accessed: 2024-05-22.

[12] Clark, S., "A Japanese spacecraft faceplanted on the Moon and lived to tell the tale," , 2024. URL https://arstechnica.com/space/2024/01/a-japanese-spacecraft-faceplanted-on-the-moon-and-lived-to-tell-the-tale/, Accessed: 2024-05-22.

[13] Betts, J. T., *Practical Methods for Optimal Control and Estimation Using Nonlinear Programming*, 2nd ed., Advances in Design and Control, SIAM, 2010. https://doi.org/10.1137/1.9780898718577.

[14] Dueri, D., Mao, Y., Mian, Z., Ding, J., and Açıkmeşe, B., "Trajectory optimization with inter-sample obstacle avoidance via successive convexification," *2017 IEEE 56th Annual Conference on Decision and Control (CDC)*, IEEE, 2017, pp. 1150–1156. https://doi.org/10.1109/CDC.2017.8263811.

[15] Breger, L., and How, J. P., "Safe Trajectories for Autonomous Rendezvous of Spacecraft," *Journal of Guidance, Control, and Dynamics*, Vol. 31, No. 5, 2008, p. 1478–1489. https://doi.org/10.2514/1.29590.

[16] Elango, P., Luo, D., Kamath, A. G., Uzun, S., Kim, T., and Açıkmeşe, B., "Successive Convexification for Trajectory Optimization with Continuous-Time Constraint Satisfaction," , 2024. https://doi.org/10.48550/arXiv.2404.16826.

[17] Teo, K. L., and Goh, C., "A simple computational procedure for optimization problems with functional inequality constraints," *IEEE Transactions on Automatic Control*, Vol. 32, No. 10, 1987, pp. 940–941. https://doi.org/10.1109/tac.1987.1104471.

[18] Buckner, S. C., Shaffer, J., Carson, J. M., Johnson, B. J., Sostaric, R. R., and Açıkmeşe, B., "Constrained Visibility Guidance for Terrain Scanning using 6-DOF Sequential Convex Programming," *AIAA SciTech 2024 Forum*, American Institute of Aeronautics and Astronautics, 2024. https://doi.org/10.2514/6.2024-1759.

[19] Malyuta, D., and Açıkmeşe, B., "Lossless Convexification of Optimal Control Problems with Semi-continuous Inputs," *IFAC-PapersOnLine*, Vol. 53, No. 2, 2020, p. 6843–6850. https://doi.org/10.1016/j.ifacol.2020.12.341.

[20] Uzun, S., Açıkmeşe, B., and Carson III, J. M., "Sequential Convex Programming for 6-DoF Powered Descent Guidance with Continuous-Time Compound State-Triggered Constraints," *AIAA SciTech 2025 Forum*, American Institute of Aeronautics and Astronautics, 2025.

[21] Kamath, A. G., Elango, P., Yu, Y., Mceowen, S., Chari, G. M., Carson, J. M., III, and Açıkmeşe, B., "Real-Time Sequential Conic Optimization for Multi-Phase Rocket Landing Guidance," *IFAC-PapersOnLine*, Vol. 56, No. 2, 2023, pp. 3118–3125. https://doi.org/10.1016/j.ifacol.2023.10.1444.

[22] Reynolds, T. P., Szmuk, M., Malyuta, D., Mesbahi, M., Açıkmeşe, B., and Carson III, J. M., "Dual Quaternion-Based Powered Descent Guidance with State-Triggered Constraints," *Journal of Guidance, Control, and Dynamics*, Vol. 43, No. 9, 2020, pp. 1584–1599. https://doi.org/10.2514/1.G004536.

[23] Kamath, A. G., Elango, P., Mceowen, S., Yu, Y., Carson III, J. M., Mesbahi, M., and Açıkmeşe, B., "Customized real-time first-order methods for onboard dual quaternion-based 6-DoF powered-descent guidance," *AIAA SciTech 2023 Forum*, American Institute of Aeronautics and Astronautics, Reston, Virginia, 2023. https://doi.org/10.2514/6.2023-2003.

[24] Lu, P., and Sandoval, S. A., "Abort Guidance during Powered Descent for Crewed Lunar Missions," *AIAA SciTech 2021 Forum*, American Institute of Aeronautics and Astronautics, 2021. https://doi.org/10.2514/6.2021-0505.

[25] Paluszek, M., *ADCS-Spacecraft Attitude Determination and Control*, Elsevier, 2023. https://doi.org/10.1016/C2021-0-00544-7.

[26] Simplício, P., Marcos, A., and Bennani, S., "Reusable Launchers: Development of a Coupled Flight Mechanics, Guidance, and Control Benchmark," *Journal of Spacecraft and Rockets*, Vol. 57, No. 1, 2020, p. 74–89. https://doi.org/10.2514/1.a34429.

[27] "MOSEK Cookbook 3.3.0," https://docs.mosek.com/modeling-cookbook/index.html, 2024. Accessed: 03-26-2024.

[28] Drusvyatskiy, D., and Lewis, A. S., "Error bounds, quadratic growth, and linear convergence of proximal methods," *Mathematics of Operations Research*, Vol. 43, No. 3, 2018, pp. 919–948. https://doi.org/10.1287/moor.2017.0889.

[29] Malyuta, D., Reynolds, T. P., Szmuk, M., Lew, T., Bonalli, R., Pavone, M., and Açıkmeşe, B., "Convex Optimization for Trajectory Generation: A Tutorial on Generating Dynamically Feasible Trajectories Reliably and Efficiently," *IEEE Control Systems*, Vol. 42, No. 5, 2022, pp. 40–113. https://doi.org/10.1109/MCS.2022.3187542.

[30] Berkovitz, L. D., *Optimal Control Theory*, Applied Mathematical Sciences, Springer New York, 1974. https://doi.org/10.1007/978-1-4757-6097-2.

[31] Bock, H. G., and Plitt, K. J., "A multiple shooting algorithm for direct solution of optimal control problems," *IFAC Proc. Vol.*, Vol. 17, No. 2, 1984, pp. 1603–1608. https://doi.org/10.1016/S1474-6670(17)61205-9.

[32] Chari, G. M., Kamath, A. G., Elango, P., and Açıkmeşe, B., "Fast Monte Carlo Analysis For 6-DoF Powered-Descent Guidance via GPU-Accelerated Sequential Convex Programming," *AIAA SciTech 2024 Forum*, AIAA, 2024, pp. 1–16. https://doi.org/10.2514/6.2024-1762.